Virtual Homonuclear Decoupling in Direct Detection NMR Experiments using Deep Neural Networks

Gogulan Karunanithy[1,*], Harold W Mackenzie[1], D. Flemming Hansen[1,*]

1) Department of Structural and Molecular Biology, Division of Biosciences, University College London, London, UK WC1E 6BT

To whom correspondence should be addressed:

D. Flemming Hansen; E-mail: d.hansen@ucl.ac.uk or

Gogulan Karunanithy; E-mail: g.karunanithy@ucl.ac.uk

Keywords: Artificial Intelligence, Biophysics, Machine Learning, NMR Spectroscopy, Proteins

Abstract

Nuclear magnetic resonance (NMR) experiments are frequently complicated by the presence of homonuclear scalar couplings. For the growing body of biomolecular ^{13}C-detected NMR methods, one-bond ^{13}C-^{13}C couplings significantly reduce sensitivity and resolution. The solution to this problem has typically been to perform virtual decoupling by recording multiple spectra and taking linear combinations. Here, we propose an alternative method of virtual decoupling using deep neural networks, which only requires a single spectrum and gives a significant boost in resolution while reducing the effective phase cycles of the experiments by at least a factor of two. We successfully apply this methodology to virtually decouple in-phase CON (^{13}CO-^{15}N) protein NMR spectra, ^{13}C-^{13}C correlation spectra of protein side chains, and $^{13}C_{\alpha}$-detected protein $^{13}C_{\alpha}$-^{13}CO spectra where two large homonuclear couplings are present. The deep neural network approach effectively decouples spectra with a high degree of flexibility, including in cases where existing methods fail, facilitates the use of simpler pulse sequences, and yields spectra with comparable quality to traditional virtual decoupling schemes in half the time or less.

Introduction

Traditionally, solution-state biomolecular NMR has focussed on ^{1}H detection-based methods owing to the high gyromagnetic ratio and therefore sensitivity of ^{1}H nuclei. However, over the last two decades, methods referred to as direct detection, involving the detection of ^{13}C or ^{15}N magnetisation have increasingly come to the fore[1–3]. Despite their lower intrinsic sensitivity, the absence of solvent signals, higher chemical shift dispersion of signals and favourable relaxation properties have made these direct detection methods very useful tools and offered new opportunities for elucidating the structures and behaviour of biomolecules.

One key advantage of employing direct detection is that spectra are not affected by the deleterious effects of labile ^{1}H exchange with the solvent[4]. As a result of solvent exchange, ^{1}H resonances in commonly employed ^{1}H-^{15}N backbone amide correlation experiments will sometimes be broadened beyond detection. This issue is particularly acute for intrinsically disordered proteins (IDPs), where the high degree of solvent exposure throughout the protein can lead to a significant loss of signal, particularly at physiologically relevant pH and temperatures[5,6]. Conversely, by focussing on non-labile ^{13}C and ^{15}N nuclei, approaches such as the CON experiment[7] and others can provide important insight into biomolecular behaviour, even in the presence of significant ^{1}H solvent exchange. Moreover, with respect to IDPs, where chemical shift dispersion in the ^{1}H dimension is low, using direct detection methods can also confer a significant resolution advantage[8–10].

A further advantage of ^{13}C- and ^{15}N-detected NMR experiments is that although low gyromagnetic ratio nuclei have reduced intrinsic sensitivity this also corresponds to lower intrinsic dipolar relaxation rates[11], though this may be offset to some extent by faster relaxation due to chemical shift anisotropy (CSA). We recently harnessed this property to record high resolution ^{13}C-^{13}C correlation spectra of the side chains in uniformly deuterated proteins[12]. The slow relaxation of the ^{13}C nuclei in these deuterated systems means that spectra can be recorded on even relatively large proteins, providing a uniquely detailed insight into the structure and dynamics of protein side chains. It has also been shown that even on protonated samples the additional steps in a pulse

sequence required to return the magnetisation back to protons and subsequent signal loss due to solvent exchange can result in {^{1}H-excite, ^{13}C-detect} sequences having higher overall sensitivity in certain cases[13,14].

Despite these clear advantages, an important issue that affects ^{13}C direct detection experiments of uniformly labelled samples is the presence of large one bond ^{13}C-^{13}C scalar couplings, typically 30-55 Hz in size, which evolve during acquisition[15]. This scalar coupling doubles, triples, or quadruples the number of peaks in the spectrum, significantly reducing their resolution and complicating interpretation. As the couplings are homonuclear, decoupling schemes can cause a range of deleterious effects in the spectra including sidebands, Bloch-Siegert shifts of the second kind and severe relaxation losses[16,17]. Consequently, the preferred method for eliminating these one-bond couplings involves virtual decoupling.

The two most common methods for virtually decoupling a single one-bond scalar coupling (a doublet) in direct detection methods are in-phase anti-phase[18] (IPAP) and spin-state selective excitation[19] (S^{3}E). In both cases two spectra are required, doubling the effective phase cycle of the experiment. For IPAP, virtual decoupling of the spectra is obtained by recording spectra with in-phase and anti-phase magnetisation detected, respectively. Taking the sum and difference of these two spectra yields two spectra each containing a peak at one component of the doublet. The peaks are subsequently centred and added together to give the final result. The S^{3}E method follows a similar scheme except that in the detected magnetisation the two components of the doublets are 90° out of phase and in the second spectrum the sign of one of the peaks is reversed. Therefore, after taking linear combinations, an additional 90° phase correction is required before the spectra are summed. For cases where two homonuclear scalar couplings are present, for example in $^{13}C_{\alpha}$ directly detected experiments where there are couplings to both ^{13}CO and $^{13}C_{\beta}$, double in-phase anti-phase (DIPAP) or double spin-state selective excitation (DS^{3}E) methods can be used to virtually decouple spectra. In this case four spectra corresponding to each permutation of the detected magnetisation are required[20–22].

All of these methods for virtual decoupling at least double the phase cycle associated with the experiment and often require additional delays and pulses in the pulse sequences to create the requisite magnetisation, causing signal loss due to relaxation and potential pulse imperfections. The S^3E methodology is slightly less onerous in terms of time (taking $0.25/^1J_{CC}$ of time rather than $0.5/^1J_{CC}$ required for IPAP) but S^3E is also less robust when there are slight variations in the scalar couplings in the spectrum. An alternative method of virtual decoupling that avoids these disadvantages is to use a signal processing algorithm that produces the decoupled spectrum from one recorded coupled spectrum. Several methods for virtual decoupling by deconvolution have been developed, most notably deconvolution with maximum entropy reconstruction[23–25]. However, despite the potential benefits associated with decoupling via signal processing, methods based on taking linear combinations of spectra have still been preferred.

Recently, we demonstrated that a deep neural network (DNN) based on dilated convolutional layers, FID-Net, could be trained to perform a variety of transformations on time domain NMR data including reconstructing non-uniformly sampled (NUS) spectra[26]. Building on this idea, we show here that FID-Net can be trained to decouple directly detected spectra using a single spectrum. We apply this methodology to ^{13}C-detected protein CON spectra and ^{13}C-^{13}C spectra of protein side chains to decouple spectra on the basis of the in-phase component of the experiment alone and demonstrate comparable spectral quality to an IPAP decoupled spectrum recorded in double the time. We further apply the methodology to $^{13}C_\alpha$-detected $^{13}C_\alpha$-^{13}CO protein spectra showing the applicability of the method to cases where one or two coupling constants are present, facilitating the use of simpler pulse sequences and providing superior decoupling performance to existing DIPAP methods.

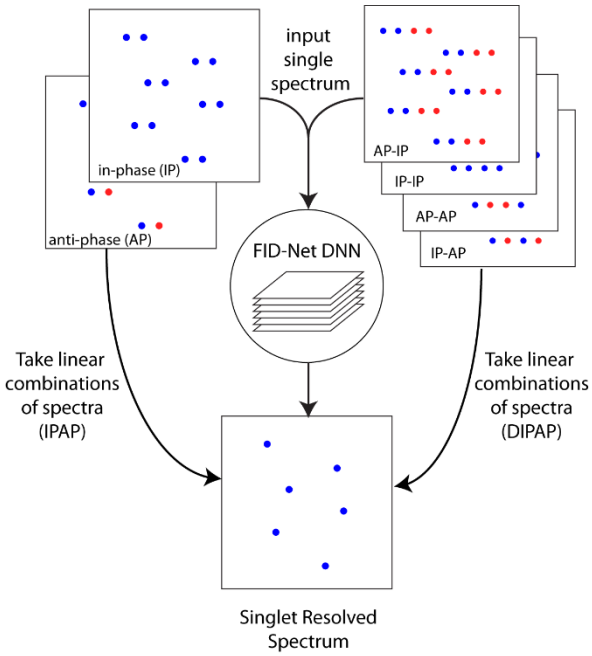

Figure 1. Schematic comparison of traditional and FID-Net based methods for virtual decoupling. Traditional methods, such as IPAP and DIPAP, require the acquisition of multiple spectra and taking linear combinations to yield a singlet resolved spectrum. Conversely, FID-Net based DNNs can be trained to decouple spectra with one or two couplings using a single spectrum.

Results

Deep Neural Network Architecture

We employed the FID-Net architecture[26] for our DNNs and here only provide a brief outline of its features. When using a DNN to model time-domain NMR data (FIDs; free induction decays) a key challenge to overcome is that information on the resonating nuclei is not localised to a specific part of an FID but rather contained over its entire length. Consequently, in order to analyse and manipulate this kind of data it is necessary for a DNN to pick up on both short- and long-range patterns within the data. In FID-Net this is achieved using stacked convolutional layers with different dilation rates[27] (Fig S1). A dilation refers to a skipped point in a convolution and by stacking convolutions with increasing dilation it is possible to create what is approximately a single convolutional layer with a very large kernel size but with much higher efficiency.

Three FID-Net based DNNs were trained to perform virtual decoupling of ^{13}C-^{13}C correlation spectra of protein side chains, ^{13}CO-^{15}N spectra and $^{13}C_{\alpha}$-^{13}CO protein correlation spectra. All the networks were trained exclusively on synthetic data and subsequently tested on experimentally acquired data (full training details are provided in the Supplementary Material).

Application to protein side chain correlation spectra

Selective pulses can be used to obtain high resolution ^{13}C-^{13}C spectra of side chains in uniformly [^{2}H,^{13}C] isotopically labelled proteins[12]. This experiment is reliant on amino acids containing a 'terminal' side chain ^{13}C resonance ($^{13}C_t$) that is directly coupled to only one other 'penultimate' ^{13}C nucleus ($^{13}C_p$) with a significantly different chemical shift distribution. The scalar coupling between $^{13}C_t$ and $^{13}C_p$ (~35 Hz) evolves during the direct acquisition period resulting in a doublet. In the original implementation this coupling was resolved using the traditional IPAP method.

In Figure 2 the performance of DNN-decoupling using the FID-Net architecture is compared with the traditional decoupling IPAP method for ^{13}C-^{13}C correlation maps of the 18 kDa protein T4 Lysozyme (T4L). Panels (A) and (B) of the figure show the results of decoupling the valine $^{13}C_{\gamma 1,2}$-$^{13}C_{\beta}$ and isoleucine $^{13}C_{\delta 1}$-$^{13}C_{\gamma 1}$ spectra, respectively. The spectra clearly demonstrate that the FID-Net decoupling provides comparable or better decoupling than the IPAP method in half the recording time. The 1D slices taken from the spectra show that the decoupling fidelity in the FID-Net spectra is excellent, both in terms of peak positions and intensities, and the procedure works well even when several peaks are present in one slice and with low intensity peaks.

The success of the FID-Net decoupling is dependent only on the size of the scalar couplings and not the specific residue being studied. Thus, the network can also be readily applied to other sites, including arginine, lysine, valine and threonine side chains, where the size of the scalar coupling is similar[12].

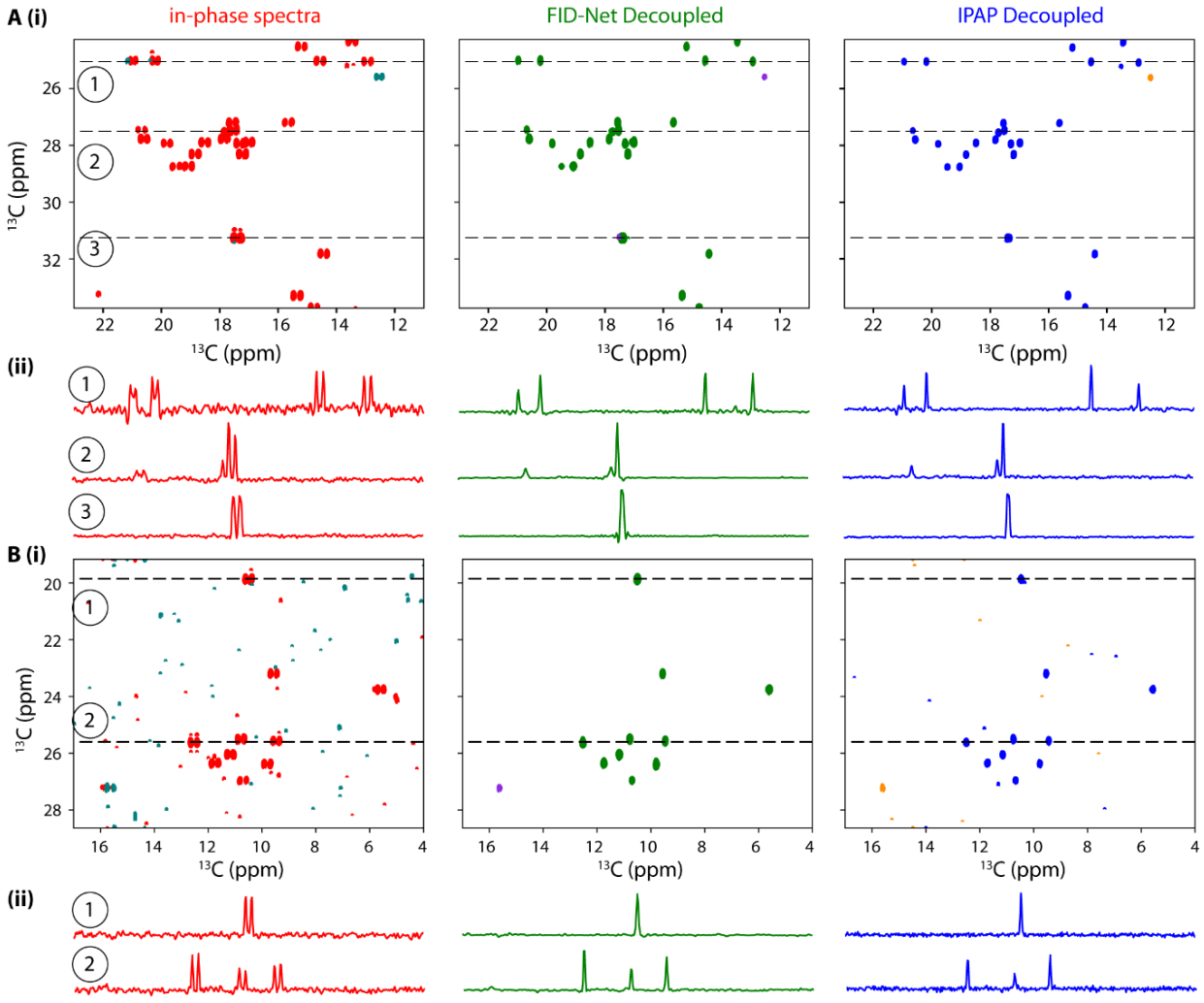

Figure 2. Comparison of in-phase (red), FID-Net decoupled (green) and IPAP decoupled (blue) $^{13}C_t$-$^{13}C_p$ spectra for the (**A**) $^{13}C_{\gamma 1,2}$-$^{13}C_\beta$ valine and (**B**) $^{13}C_{\delta 1}$-$^{13}C_{\gamma 1}$ isoleucine spectra of [^{2}H,^{13}C] labelled T4L recorded at 14.1 T (600 MHz) and at a temperature of 298 K. For all spectra, the alternative colour indicates negative contour levels. The FID-Net DNN carries out the decoupling procedure using only the in-phase spectra while the IPAP procedure uses both the in-phase and anti-phase (not shown) spectra. 1D slices from the indicated regions of each spectra are shown in (ii). For 2D spectra, FID-Net decoupled and IPAP decoupled spectra are shown at the same contour levels relative to the maximum signal, facilitating comparisons of signal-to-noise between the spectra.

Application to protein CON Spectra

While benchmarks on the $^{13}C_t$-$^{13}C_p$ spectra show the potential of a DNN-based approach for virtual decoupling, each of these spectra has relatively few peaks that are well dispersed. To assess the robustness of the DNN-based decoupling method we switched our attention to the CON class of experiments that provide ^{13}CO-^{15}N correlations maps[7]. Unlike for the $^{13}C_t$-$^{13}C_p$ spectra where only one or two types of amino acids can be characterised in each spectrum, severely restricting the total number of signals in the spectrum, a CON experiment simultaneously reports on all backbone residues. Therefore, the spectrum will contain many more cross-peaks and a much greater probability of overlap between resonances, making the task of virtual homonuclear decoupling substantially more demanding.

In Figure 3 we compare the results of decoupling using the FID-Net method and IPAP for CON spectra of the proteins ubiquitin and α-synuclein. In both cases we see that the DNN-approach is able to decouple the spectra effectively and shows favourable performance compared to the IPAP approach, even in the presence of substantially more cross-peaks. Notably, even when the components of different doublets are overlapping the DNN is able to correctly decouple the peaks. As shown in Figures S2 and S3 all expected cross-peaks are recovered in the FID-Net decoupled spectra for both proteins. The ability to virtually decouple CON spectra containing large numbers of peaks further demonstrates the robustness of the DNN decoupling approach and its viability as an alternative to IPAP or S^3E methods. With the use of DNN decoupling it is also possible to produce these spectra in half the time of the IPAP approach given that only the in-phase component is used.

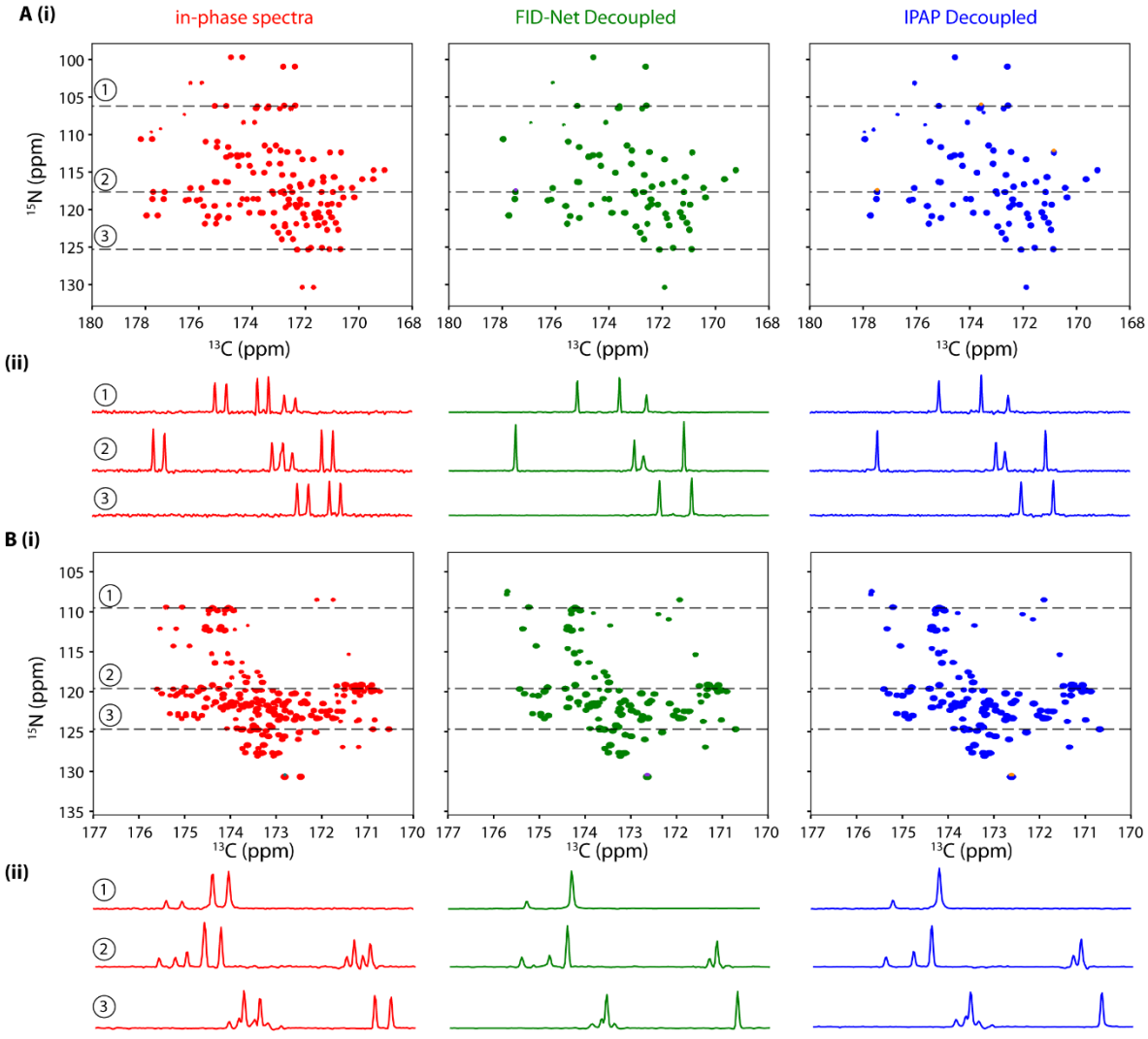

Figure 3. Comparison of in-phase (red), FID-Net decoupled (green) and IPAP decoupled (blue) CON spectra for **(A)** ubiquitin and **(B)** α-synuclein. **(ii)** 1D slices for each of the spectra from the indicated regions. Full acquisition details for the spectra are provided in the supporting information.

An important point to address in both the CON and IPAP FID-Net decoupled spectra is that of thermal noise in the spectrum. During training of the DNN random normal noise with standard deviation between 0.001 and 0.15 times the maximum signal is added to the input signal, with the network aiming to produce an output that is denoised. The results shown in Fig 2 and 3 (also Fig S2 and S3) show that the thermal noise in the spectra is suppressed to a large degree. A key

advantage the neural network has in attempting to denoise the spectra is that all signals in the input spectra have a similar signature, that is, in the time domain they are all cosine modulated with a coupling constant in a specific range. This makes the task of the neural network in trying to effectively disentangle signals from noise much more straightforward than when the signal can have arbitrary properties.

To gain additional insight into the performance of the neural network on experimental data, varying amounts of random noise was added to the most challenging spectrum, the CON spectrum of α-synuclein, and the decoupling was assessed for both DNN-based decoupling and IPAP decoupling. The results of this assessment are shown in Fig 4. It is seen that the DNN-based method remains robust even in the presence in large amounts of noise. Specifically, peaks that remain clearly distinguishable above the noise remain well decoupled and the underlying noise in the spectra is kept minimal – particularly in comparison to the IPAP approach. It is clear, however, that when a cross-peak is close in intensity to the noise it can be suppressed in the DNN-approach, resulting in it missing from the spectrum or having a distorted peak shape and/or intensity. Overall, we find that the DNN-approach has a preference for peaks with very low signal-to-noise to not be present in the decoupled spectrum as opposed to generating artefacts. In the presence of large amounts of noise however, the neural network can also produce spurious peaks as shown in middle-right panel of Fig 4. The maximum size of these artefacts is no greater than the noise in the input spectrum.

The non-linear nature of the transformation performed by the deep neural network means that the noise in the resulting spectra is no longer useful in judging the reliability of signals in the spectrum. To gain greater quantitative insight into the quality of the virtual decoupling, synthetic spectra were created and then processed with FID-Net and IPAP decoupling schemes at different noise levels (Fig S6-S9). While the synthetic data cannot fully capture the range of artefacts encountered in experiments, using synthetic spectra means that the ground truth is known, which in turn allows for a quantitative assessment using NUScon[28] metrics. The assessment demonstrates that FID-Net decoupling can yield comparable quality spectra to IPAP decoupling in terms of peak

identification, position and intensity in half the time (as it requires only the in-phase magnetisation component).

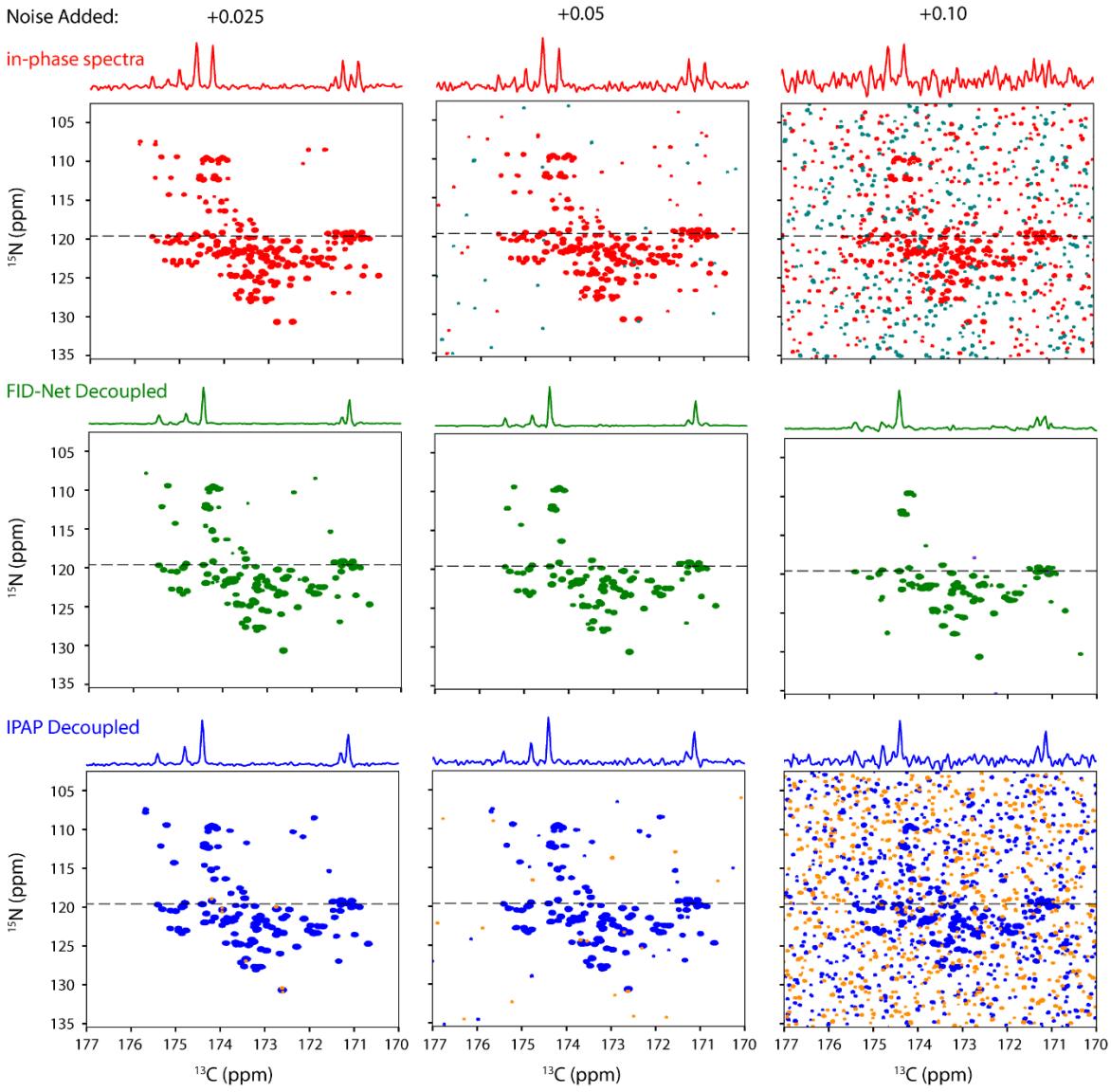

Figure 4. Comparing the outcome of virtual decoupling CON spectra of α-synuclein following the addition of random normal noise with standard deviations of 0.025, 0.05 and 0.10 times the maximum signal. The FID-Net and IPAP decoupled spectra are plotted at the same contour level to allow for comparisons.

Application to protein $^{13}C_{\alpha}$-detected Spectra

Finally, we turned our attention to training a DNN to decouple $^{13}C_{\alpha}$ directly detected spectra. In this case the signals in the resulting spectra are modulated by two couplings, that is, between $^{13}C_{\alpha}$ and ^{13}CO nuclei (~55 Hz) and between $^{13}C_{\alpha}$ and $^{13}C_{\beta}$ nuclei (~35 Hz). The latter coupling is missing for glycine residues where there is no $^{13}C_{\beta}$, adding a further level of complexity. These experiments are usually virtually decoupled using a DIPAP or DS^{3}E scheme requiring linear combinations from four spectra that include all permutations of the acquired magnetisation in-phase and anti-phase to the two couplings[20–22].

Even with this long effective phase cycle, the decoupling performance of the DIPAP or DS^{3}E schemes is incomplete. This is because these schemes rely on band-selective inversion of $^{13}C_{\beta}$ resonances. In the case of threonine and serine resonances, where the $^{13}C_{\alpha}$ and $^{13}C_{\beta}$ chemical shifts overlap, the decoupling performance is poor. Moreover, cross-peaks from glycine residues are also distorted by this process.

Using the DNN approach illustrated here overcomes these issues. Since there is no requirement to record multiple spectra and attempt selective inversions of $^{13}C_{\beta}$ resonances, the pulse sequence used to record a 2D $^{13}C_{\alpha}$-detected spectrum can be significantly simplified (Fig S5). Removing the DIPAP (or DS^{3}E) element from this pulse sequence saves 14 ms (or 7 ms), which improves signal to noise at the start of acquisition and prevents distortions where $^{13}C_{\beta}$ resonances cannot be properly refocussed. Consequently, the resultant input spectrum for the DNN contains peaks that are anti-phase with respect to the ^{13}CO coupling and in-phase respect to $^{13}C_{\beta}$ where this is present (Fig 5). The DNN was trained to decouple these spectra to yield singlet resolved resonances in a single shot analysis.

A comparison of the FID-Net and DIPAP decoupling approaches applied to a sample of ubiquitin is shown in Fig 5. The FID-Net decoupled spectra clearly provide superior decoupling performance compared to the DIPAP approach, avoiding many of the peak distortions. An additional example of this approach is the decoupling of a $^{13}C_{\alpha}$-detected spectrum of T4 Lysozyme

shown in Fig S4. Notably, the DNN is not only able to decouple the {anti-phase, in-phase} modulated peaks associated with the majority of residues, but also the glycine peaks and those associated with protein side chains that are distorted in the DIPAP spectrum. Specifically, peaks associated with asparagine and glutamate side chains are also readily decoupled in the FID-Net decoupled spectra but distorted by the DIPAP procedure.

A quantitative assessment was performed of the performance of the $^{13}C_{\alpha}$ decoupling network using NUScon[28] metrics at different noise levels (Fig S10-S13). The quantitative assessment demonstrates the high fidelity with which the FID-Net DNN decouples $^{13}C_{\alpha}$-detected spectra. Compared to the network for decoupling in-phase spectra such as CON, the linearity of decoupled intensities is slightly lower for decoupling of $^{13}C_{\alpha}$-detected spectra, which reflects the fact that the signals in this case are sine- rather than cosine-modulated, meaning that the intensity of the first points in the output FIDs (approximately 9 ms) must be extrapolated by the DNN.

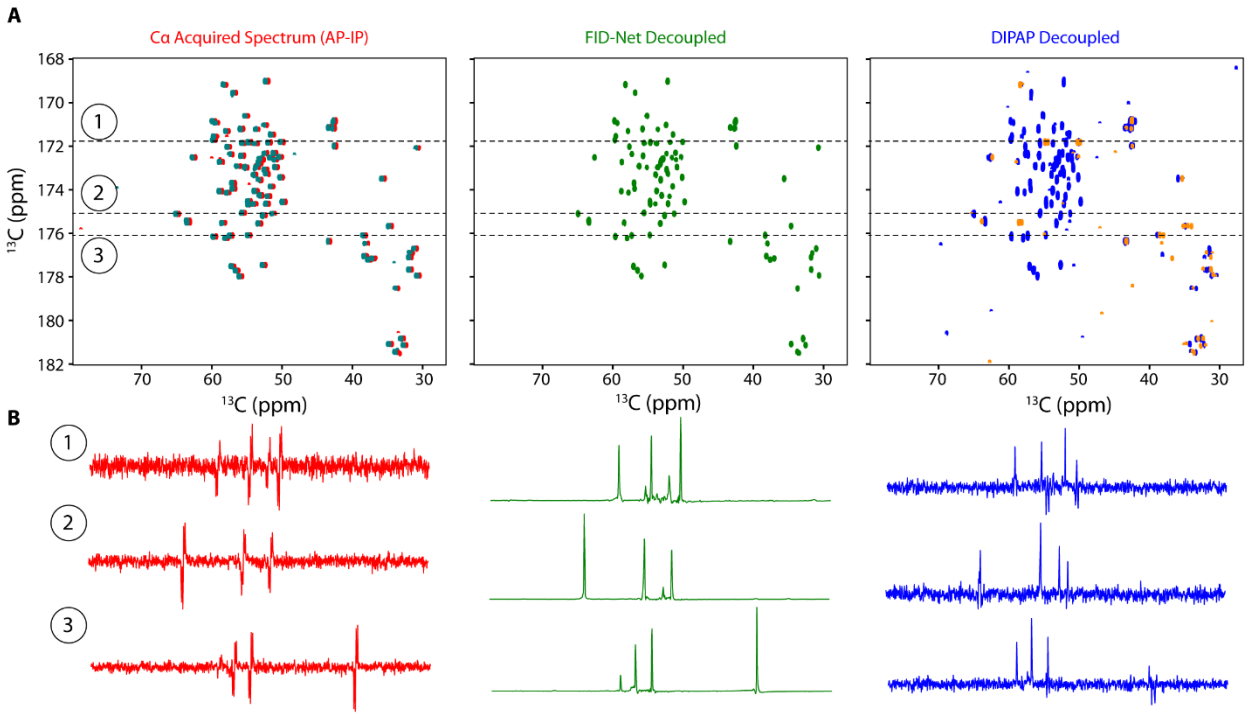

Figure 5 (A) Comparison of antiphase,in-phase (AP-IP) (red), FID-Net decoupled (green) and DIPAP decoupled (blue) $^{13}C_{\alpha}$-^{13}CO spectra from a 0.5 mM ubiquitin sample at 298 K. In each spectrum the alternative colour indicates negative contour levels. **(B)** 1D slices for each of the spectra from the indicated regions. Full acquisition details for the spectra are provided in the supporting information.

Discussion

The DNN approach introduced here represents a flexible and effective tool for performing virtual decoupling of directly detected experiments. A key guiding principle in the design of our FID-Net architecture is that a single network should be generalisable to a range of situations – a network that is able to do this should have good robustness. All the results shown above are from one architecture and only three sets of DNNs parameters: one set for $^{13}C_t$-$^{13}C_p$ spectra, one for CON spectra and one for $^{13}C_\alpha$-detected spectra. This versatility means that there is no requirement for the end user to perform any further training provided that the experimental parameters do not deviate too far from those used in training and the methodology can therefore easily be implemented for a broad range of applications.

The DNN method provides effective and robust decoupling meaning that singlet-resolved $^{13}C_t$-$^{13}C_p$ and CON spectra of similar quality to IPAP decoupling are obtained in half the time. The DNN for decoupling CON spectra was trained on spectra with up to 200 cross-peaks per 2D plane. For decoupling CON spectra with more signals with the DNN we recommend extending the acquisition time in the indirect ^{15}N dimension, which will lead to a higher resolution in the indirect dimension and thus fewer signals per slice in the ^{13}CO dimension. The assessment in Supplementary Material indicate that robust decoupling can be obtained with the DNN method as long as the signal-to-noise of peaks in the input spectrum is above ~2.5. For samples where signal-to-noise is very low the IPAP method is likely preferable as it increases signal to noise by a factor of two compared to the in-phase spectrum alone while also removing couplings.

When the chemical shift difference between the active and passive spin is large, for example in CON spectra, an alternative method for decoupling ^{13}C-^{13}C couplings is provided by the LOW-BASHD method. In LOW-BASHD decoupling of CON spectra, $^{13}C_\alpha$ couplings are refocussed during acquisition[17,29] and the pulses used for decoupling are optimised to minimise first order effects of Bloch-Siegert shifts of the second kind. However, the LOW-BASHD method relies on large chemical shift differences and knowledge of the chemical shift of the coupled spin. A key advantage of the DNN decoupling approach over any experimental scheme for decoupling is that the decoupling by the DNN is completely independent of the resonance frequency of the coupled

spin. Thus, while a side chain resonance may fall outside the effective decoupling range of the LOW-BASHD method, such a scenario will not pose a problem for the DNN method provided that the coupling constant is in the expected range. This flexibility also allows the DNN methodology to be deployed in situations such as in $^{13}C_t$-$^{13}C_p$ spectra where implementation of the LOW-BASHD methods would be difficult or impossible.

The extension of the DNN approach to effectively decouple $^{13}C_\alpha$-detected spectra represents a significant advance over existing virtual decoupling methods based on taking linear combinations (e.g. DIPAP) as well as signal processing methods such as deconvolution with maximum entropy reconstruction[23]. Experimental approaches for fully decoupling $^{13}C_\alpha$-detected spectra, potentially based on BASHD[30,31], would likely suffer from reduced signal intensity, distorted peaks for glycine, serine, and threonine, and be highly demanding in terms of probe power requirements. The application of the DNN methodology to $^{13}C_\alpha$-detected spectra further demonstrates how the DNN decoupling method is not affected by the chemical shift distributions of coupled nuclei, which must be considered for other experimental decoupling schemes, as only the size and phase of the couplings is important.

Conclusion

A perennial challenge facing many ^{13}C-direct detect NMR experiments is the presence of homonuclear scalar couplings that evolve during acquisition. While virtual decoupling methods involving taking linear combinations of spectra can address this issue, this may result in a more complicated pulse sequence, distort some peaks and increase the effective phase cycle of the experiment by at least a factor of two. Here we have demonstrated how the FID-Net architecture can be trained to effectively decouple a range of ^{13}C-detected experiments on the basis of a single spectrum. This methodology can be simply implemented as part of the spectral processing procedure, offering substantial potential time savings and yielding high quality spectra. Having the DNN analysis tool also opens up a new perspective within the design of pulse sequences and for these to be rethought and simplified. In the case of $^{13}C_\alpha$-^{13}CO spectra shown here the final 'DIPAP block' can be removed, resulting in cleaner spectra with higher sensitivity, overall creating a virtuous cycle between the experiment and the analysis method. The methodology presented here

adds to the growing applications of deep learning and artificial intelligence for analysing NMR data and paves the way for forthcoming developments to transform the way in which NMR spectroscopy data are recorded, processed, and analysed.

Associated Content

The supporting material is available free of charge via the Internet at http://pubs.acs.org.

- Protein production and purification protocols. Parameters used for NMR experiments. Protocols for making DNN training data and training DNNs as well as visualization of FID-Net architecture. Spectra showing recovery of peaks following virtual decoupling and performance of DNNs for virtually decoupling synthetic data.

Author Information

Corresponding Authors

* D. Flemming Hansen; Department of Structural and Molecular Biology, Division of Biosciences, University College London, London, United Kingdom, WC1E 6BT E-mail: d.hansen@ucl.ac.uk.

* Gogulan Karunanithy; Department of Structural and Molecular Biology, Division of Biosciences, University College London, London, United Kingdom, WC1E 6BT E-mail: g.karunanithy@ucl.ac.uk.

Authors

Harold W Mackenzie - Department of Structural and Molecular Biology, Division of Biosciences, University College London, London, United Kingdom, WC1E 6BT

Funding Sources

This research is supported by the Biotechnology and Biological Sciences Research Council (BBSRC) (ref: BB/T011831/1 and BB/R000255/1) as well as the Wellcome Trust (ref: 101569/Z/13/Z).

Notes

Code (python) for virtually decoupling CON, $^{13}C_t$-$^{13}C_p$ and $^{13}C_\alpha$-detected spectra using FID-Net (including pre-trained networks and examples) is available on GitHub: https://github.com/gogulan-k/FID-Net. The authors declare no competing financial interest.

Acknowledgements

This study made use of NMRbox: National Center for Biomolecular NMR Data Processing and Analysis[28], a Biomedical Technology Research Resource (BTRR), which is supported by NIH grant P41GM111135 (NIGMS). The BBSRC (BB/R000255/1) and Wellcome Trust (ref 101569/z/13/z) are acknowledged for supporting the biomolecular NMR facility at University College London. This work was supported by the Francis Crick Institute through provision of access to the Scientific Computing STP and the Crick data Analysis and Management Platform (CAMP). The Francis Crick Institute receives its core funding from Cancer Research UK (FC010233), the UK Medical Research Council (FC010233), and the Wellcome Trust (FC010233).

References

[1] W. Bermel, I. C. Felli, R. Kümmerle, R. Pierattelli, *Concepts Magn. Reson. Part A Bridg. Educ. Res.* **2008**, *32*, 183–200.

[2] Z. Serber, C. Richter, D. Moskau, J. M. Böhlen, T. Gerfin, D. Marek, M. Häberli, L. Baselgia, F. Laukien, A. S. Stern, et al., *J. Am. Chem. Soc.* **2000**, *122*, 3554–3555.

[3] K. Takeuchi, H. Arthanari, M. Imai, G. Wagner, I. Shimada, *J. Biomol. NMR* **2016**, *64*, 143–151.

[4] M. Bastidas, E. B. Gibbs, D. Sahu, S. A. Showalter, *Inc. Concepts Magn Reson Part A* **2015**, *44*, 54–66.

[5] E. B. Gibbs, R. W. Kriwacki, *Methods* **2018**, *138–139*, 39–46.

[6] S. Gil, T. Hošek, Z. Solyom, R. Kümmerle, B. Brutscher, R. Pierattelli, I. C. Felli, *Angew. Chemie Int. Ed.* **2013**, *52*, 11808–11812.

[7] W. Bermel, I. Bertini, I. C. Felli, R. Kümmerle, R. Pierattelli, *J. Magn. Reson.* **2006**, *178*, 56–64.

[8] E. C. Cook, G. A. Usher, S. A. Showalter, *Methods Enzymol.* **2018**, *611*, 81–100.

[9] I. C. Felli, R. Pierattelli, *J. Magn. Reson.* **2014**, *241*, 115–125.

[10] K. Takeuchi, H. Arthanari, I. Shimada, G. Wagner, *J. Biomol. NMR* **2015**, *63*, 323–331.

[11] S. Chhabra, P. Fischer, K. Takeuchi, A. Dubey, J. J. Ziarek, A. Boeszoermenyi, D. Mathieu, W. Bermel, N. E. Davey, G. Wagner, et al., *Proc. Natl. Acad. Sci. U. S. A.* **2018**, *115*, E1710–E1719.

[12] R. B. Pritchard, D. F. Hansen, *Nat. Commun.* **2019**, *10*, DOI 10.1038/s41467-019-09743-4.

[13] W. Bermel, I. Bertini, I. C. Felli, R. Pierattelli, *J. Am. Chem. Soc.* **2009**, *131*, 15339–15345.

[14] G. Karunanithy, J. Reinstein, D. F. Hansen, *J. Phys. Chem. Lett.* **2020**, *11*, 5649–5654.

[15] W. Bermel, I. Bertini, I. C. Felli, M. Piccioli, R. Pierattelli, *Prog. Nucl. Magn. Reson. Spectrosc.* **2006**, *48*, 25–45.

[16] F. Bloch, A. Siegert, *Phys. Rev.* **1940**, *57*, 522–527.

[17] J. Ying, F. Li, J. H. Lee, A. Bax, *J. Biomol. NMR* **2014**, *60*, 15–21.

[18] M. Ottiger, F. Delaglio, A. Bax, *J. Magn. Reson.* **1998**, *131*, 373–378.

[19] M. D. Sørensen, A. Meissner, O. W. Sørensen, *J. Biomol. NMR* **1997**, *10*, 181–186.

[20] L. Duma, S. Hediger, A. Lesage, L. Emsley, *J. Magn. Reson.* **2003**, *164*, 187–195.

[21] W. Bermel, I. Bertini, L. Duma, I. C. Felli, L. Emsley, R. Pierattelli, P. R. Vasos, *Angew. Chemie - Int. Ed.* **2005**, *44*, 3089–3092.

[22] W. Bermel, I. Bertini, I. C. Felli, M. Matzapetakis, R. Pierattelli, E. C. Theil, P. Turano, *J. Magn. Reson.* **2007**, *188*, 301–310.

[23] N. Shimba, A. S. Stern, C. S. Craik, J. C. Hoch, V. Dötsch, *J. Am. Chem. Soc.* **2003**, *125*, 2382–2383.

[24] Z. Serber, C. Richter, V. Dötsch, *ChemBioChem* **2001**, *2*, 247–251.

[25] M. A. Delsuc, G. C. Levy, *J. Magn. Reson.* **1988**, *76*, 306–315.

[26] G. Karunanithy, D. F. Hansen, *J. Biomol. NMR* **2021**, *75*, 179–191.

[27] A. van den Oord, S. Dieleman, H. Zen, K. Simonyan, O. Vinyals, A. Graves, N. Kalchbrenner, A. Senior, K. Kavukcuoglu, *arXiv* **2016**, 1–15.

[28] M. W. Maciejewski, A. D. Schuyler, M. R. Gryk, I. I. Moraru, P. R. Romero, E. L. Ulrich, H. R. Eghbalnia, M. Livny, F. Delaglio, J. C. Hoch, *Biophys. J.* **2017**, *112*, 1529–1534.

[29] J. O. Struppe, C. Yang, Y. Wang, R. V. Hernandez, L. M. Shamansky, L. J. Mueller, *J. Magn. Reson.* **2013**, *236*, 89–94.

[30] J. Ying, J. Roche, A. Bax, *J. Magn. Reson.* **2014**, *241*, 97–102.

[31] R. Brüschweiler, C. Griesinger, O. W. Sørensen, R. R. Ernst, *J. Magn. Reson.* **1988**, *78*, 178–185.

Table of Contents artwork